Thermal Emission from H II Galaxies: Discovering the Youngest Systems

Article *in* The Astrophysical Journal · January 2007

DOI: 10.1086/509105 · Source: arXiv

4 authors, including:

Henrique Schmitt
United States Naval Research Laboratory
257 PUBLICATIONS **3,980** CITATIONS
SEE PROFILE

Elena Terlevich
Instituto Nacional de Astrofísica, Óptica y Elect…
143 PUBLICATIONS **1,261** CITATIONS
SEE PROFILE

Roberto Terlevich
Instituto Nacional de Astrofísica, Óptica y Elect…
478 PUBLICATIONS **13,950** CITATIONS
SEE PROFILE

Thermal Emission from HII Galaxies: Discovering the Youngest Systems

D. Rosa-González

Instituto Nacional de Astrofísica Optica y Electrónica. Luis Enrique Erro No. 1. Tonantzintla, Puebla, C.P. 72840, México; danrosa@inaoep.mx.

H. R. Schmitt

Remote Sensing Division, Code 7210, Naval Research Laboratory, 4555 Overlook Avenue, Washington, DC 20375, USA; and
Interferometrics, Inc., 13454 Sunrise Valley Drive, Suite 240, Herndon, VA 20171, USA; henrique.schmitt@nrl.navy.mil.

and

E. Terlevich[1] and R. Terlevich[1]

Instituto Nacional de Astrofísica Optica y Electrónica. Luis Enrique Erro No. 1. Tonantzintla, Puebla, C.P. 72840, México; eterlevi@inaoep.mx, rjt@inaoep.mx.

ABSTRACT

We studied the radio properties of very young massive regions of star formation in HII galaxies, with the aim of detecting episodes of recent star formation in an early phase of evolution where the first supernovae start to appear. Our sample consists of 31 HII galaxies, characterized by strong Hydrogen emission lines, for which low resolution VLA 3.5 cm and 6 cm observations were obtained. We complemented these observations with archival data at 20 cm. We found that the radio spectral energy distribution (SED) has a range of behaviours; 1) there are galaxies where the SED is characterized by a synchrotron-type slope, 2) galaxies with a thermal slope, and, 3) galaxies with possible free-free absorption at long wavelengths. The latter SEDs were found in a few galaxies (e.g. UM 533, Tololo 1223-388) and represent a signature of heavily embedded massive star clusters closely related to the early stages of massive star formation.

Based on the comparison of the star formation rates (SFR) determined from the recombination lines and those determined from the radio emission we find

[1]Visiting Fellow, IoA, Cambridge.

that SFR(Hα) is on average five times higher than SFR(1.4 GHz). We confirm this tendency by comparing the ratio between the observed flux at 20 cm and the expected one, calculated based on the Hα star formation rates, both for the galaxies in our sample and for normal ones. This analysis shows that this ratio is a factor of 2 smaller in our galaxies than in normal ones, indicating that they fall below the FIR/radio correlation. This result is further confirmed by the detection of high q-parameter values (the ratio of infrared to radio fluxes) in a few sources. These results suggest that the emission of these galaxies is dominated by a recent and massive star formation event in which the first supernovae (SN) just started to explode. This indicates that the radio emission is most likely dominated by free-free continuum, and that the emission at low frequencies may be optically thick, in agreement with the observed SEDs.

We combined the VLA data with age indicators based on optical observations (e.g. equivalent width of Hβ) together with the ratio between the far infrared and the radio continuum fluxes and proposed an evolutionary scenario to explain the observed trends. We conclude that the systematic lack of synchrotron emission in those systems with the largest equivalent width of Hβ can only be explained if those are young starbursts of less than 3.5Myr of age, i.e. before the first type II SNe start to explode.

Subject headings: galaxies: evolution, radio continuum: galaxies

1. Introduction

One of the outstanding problems in the study of starburst galaxies is understanding how massive stellar clusters (MSC) form and evolve. Most of what is known about MSC comes from the study of relatively old objects, since they evolve fast and can be heavily embedded in their earlier stages, thus being difficult to detect (Johnson 2004). Recent attempts using radio observations have been successful in the detection of several of these embedded sources in nearby starburst galaxies. During the early stages of evolution, very young star clusters should either lack or have a deficit of synchrotron emission, being dominated by free-free radio emission. Given that the synchrotron emission observed in starbursts is due to supernova activity, it is a direct tracer of the end of the evolution of massive stars ($M \geq 8\,M_\odot$). In the case of a coeval star formation burst, the first type II SNe appear after only 3.5 Myr and last until the $8\,M_\odot$ stars explode at around 40 Myr. Consequently, the lack of synchrotron emission is a good indicator of very young clusters.

Recent radio observations (e.g. Turner, Beck, & Ho 2000; Johnson et al. 2001; Johnson

et al. 2003; Cannon & Skillman 2004) have detected in a few nearby starburst galaxies, sources with compact flat radio spectrum which can be securely identified as young star clusters. In some of the cases these authors detect an inverted spectrum at low frequencies, due to free-free absorption, indicating that the cluster still is deeply embedded in the material from which it was formed. On a more global scale, Roussel et al. (2003) detected galaxies with abnormally high infrared to radio continuum ratios, identified as nascent starbursts.

One important question is how MSC do form? Are they the product of an instantaneous event or the star formation activity lasts several Myr instead? The situation is not clear, the excellent radio-FIR correlation (e.g. Yun et al. 2001) strongly suggests that star formation, at least at galactic scales, must proceed continuously; also in a study of the statistical properties of HII galaxies we found strong indications of continuous star formation (Terlevich et al. 2004). On the other hand, the presence of strong WR features in the spectra of starbursts and HII galaxies suggests a high degree of synchronization in the formation of massive stars. The question may be solved studying the properties of a complete sample of young systems.

Although these young starbursts are known, their numbers are relatively small. The detection of a larger number of young sources is an important step in the study of the early stages of massive star formation and evolution. This will allow us to better understand their properties and environment.

For this work we have taken a different approach, which consists in determining the radio properties of a sample of HII galaxies selected because their emission line spectra indicate extreme youth. HII galaxies are low mass objects whose emission and thus most observables are dominated by a massive burst of star formation. Their optical spectrum is identical to that observed in giant HII regions like 30-Doradus in the LMC. These properties make these galaxies ideal targets for a study of integrated properties in search for features related to MSCs. The best sources can then be studied in more detail with higher resolution observations. In this sense HII galaxies are considered "young". In fact they are probably the youngest stellar systems that can be studied in any detail. The youth scenario is supported not only by the strong emission lines from ionized gas, but also by their underlying stellar continuum properties, i.e. no stellar absorptions are detected in those HII galaxies with the strongest emission lines (EW(Hβ) >150Å) and only weak hydrogen and helium and some very weak metal lines are detected on those more evolved HII galaxies (EW(Hβ) < 50Å). The lack of detection of stellar absorptions in the extreme HII galaxies is due to the fact that the optical spectrum of very young clusters is dominated by the light of massive blue supergiants close to the main sequence turn-off. The spectrum of these stars shows narrow and relatively weak absorptions of hydrogen and helium plus extremely weak metal lines.

In the case of HII galaxies (and also HII regions) the weak and narrow stellar absorptions are filled with strong emission from the ionized gas of the associated HII region making it impossible to detect directly their presence. This has been traditionally a problem for studies to derive highly precise helium abundances as required for example for primordial helium determinations (e.g. Skillman, Terlevich & Terlevich 1998). Thus very strong emission plus a "featureless" continuum is the signature of extremely young HII galaxies.

This "youth" of the HII galaxies does not imply that the whole galaxy is young, in fact the opposite is probably true given the colors of the extensions detected in some HII galaxies (Telles & Terlevich, 1997) and the simple fact that the metal content of all HII galaxies is typically around 0.1-0.2 of solar (e.g. Hoyos & Díaz 2006) implying a substantial amount of chemical evolution or astration previous to the present dominant burst. Stellar population synthesis analysis (Raimann et al. 2000a, Raimann et al. 2000b) show that there is some evidence for older stellar populations in these sources, albeit at a very low level, again confirming that their emission is in fact dominated by recent star formation.

Thus "young" and "age" in this context refers to the present burst. HII galaxies could be, and probably are, much older.

Here we present the results of a study of integrated radio spectral energy distributions (SEDs) of nascent starburst candidates. We find several galaxies with flat spectrum, typical of thermal emission, or even with inverted spectra, indicating the presence of heavily embedded star clusters. With the data at hand we compare the radio and emission line (Hα,Hβ) properties of these galaxies and propose a qualitative evolutionary model.

This paper is organized in the following way. In Section 2 we describe how the sample was selected. Section 3 describes the VLA observations at 6 cm (4.9 GHz) and 3.5 cm (8.4 GHz) and the data reduction. Section 4 presents the radio SEDs, spectral indices and the proposed evolutionary model. In Section 5 we study the optical properties of the sample galaxies and calculate the SFRs obtained from the optical emission lines. In Section 6 we combined optical and radio data to discuss the nature of the selected galaxies and explore simple evolutionary scenarios. In Section 7 we estimate the FIR to radio continuum flux ratios (q parameter) and its relation to other observables to confirm the young nature of some of the observed galaxies. Finally, a summary of our results is presented in Section 8.

2. Sample Selection

Our sample selection was based on the expectation that in young starforming galaxies their most massive stars did not have enough time to evolve and explode as supernovae. In

a situation like this, these galaxies should have very little synchrotron emission (Bressan, Silva & Granato 2002). Consequently, their radio luminosities should be smaller than what one would expect to find based on the SFR measured from other indicators, like Hα.

For the current study we selected a sample from the catalog of HII galaxies by Terlevich et al. (1991; hereafter HIIG91). Based on the reddening corrected Hα fluxes of the galaxies in this catalog, we estimate their Star Formation Rates (SFR) using the relation given by Rosa-González, Terlevich and Terlevich (2002). These SFRs were then converted into radio 1.4 GHz fluxes, using the relation given by Schmitt et al. (2006). Comparing the predicted 1.4 GHz fluxes with values obtained from the NRAO/VLA Sky Survey (NVSS) catalog, we selected those galaxies which were not detected at the NVSS 5σ limit (2.5 mJy), or have an observed flux smaller than the predicted one.

Our final sample is composed of 31 galaxies which are presented in Table 1. Details about the VLA observations are described below.

3. Observations

Our observations were obtained with the VLA in 2004-Sep-01, in the early stages of the reconfiguration from D to A array. The galaxies were observed at 4.9 GHz (6 cm) and 8.4 GHz (3.5 cm), in snapshot mode, integrating for ∼10 minutes per frequency. Observations of the sources were immediately preceded and followed by ∼2 minutes observations of a phase calibrator. We used calibrators from the NRAO list, preferentially closer than 10° from the galaxies. All the observations were done in standard continuum mode with 2 IF's of 50 MHz bandwidth each, using the radio galaxies 3C 48 and 3C 286 as primary calibrators. For the sources previously observed by the VLA we used archival data to complement our observations.

The reductions followed standard AIPS techniques, which consisted of flagging bad data points, setting the flux-density scale using the primary calibrators and phase calibrating using the secondary calibrators. Since the observations happened in the early stages of the reconfiguration, most of the antennas were still in the D-configuration. Given that we are interested only in the integrated properties of these galaxies, we flagged the 6 antennas that had already been moved to the A configuration. Images were created using uniform weighting. For a few sources we compared these images with ones created using natural weighting, which is more sensitive to the extended emission, but did not find any difference. This is due to the fact that we flagged the outer antennas and were sensitive only to the large scale emission. For those sources with peak flux densities of ∼1 mJy or higher, we

interactively self-calibrate them two or three times in phase.

The noise of the images was determined in regions free from emission. The total Stokes **I** fluxes were obtained by integrating the regions brighter than 3σ above the background level. All the sources are unresolved by our observations. The errors in the flux measurements were calculated by taking into account, in quadrature, a 1.5% uncertainty in the flux calibration and Poisson noise, which usually dominates the errors. Table 1 gives the galaxies observed, the VLA project from which they were obtained and the image reconstruction beam parameters. The 1.4 GHz data were obtained from the NVSS catalog. For those galaxies that were not detected at this frequency we list the reconstruction beam of the nearest detectable source for reference.

4. Radio Spectral Energy Distribution

In Figures 1 and 2 we present the radio SEDs of the observed galaxies. The fluxes used for these Figures are presented in Table 2, where we also give the spectral indices ($\alpha, F_\nu \propto \nu^\alpha$), between 1.4 and 4.9 GHz ($\alpha_5^{1.4}$) and between 4.9 and 8.4 GHz (α_8^5), calculated using these fluxes. Figure 1 presents the galaxies that were detected at all wavelengths, while Figure 2 presents the sources for which the 1.4 GHz flux is only an upper limit. In cases like this we calculated an upper limit for $\alpha_5^{1.4}$ assuming a 1.4 GHz flux corresponding to 3 times the r.m.s. value of the NVSS image. Notice also that for some of the sources presented in Table 2 (e.g. MRK 930) we do not give information about spectral indices, even though these galaxies were detected in at least a couple of bands. This is due to the fact that different frequencies were observed with significantly different configurations. As a result, one of the frequencies was not properly sampled at short baselines, thus missing the diffuse, more extended emission. Calculating spectral indices with these data would produce meaningless results.

Analyzing the spectral slopes of the galaxies detected at 1.4 GHz we find that they have $\alpha_5^{1.4}$ values between those expected for thermal emission ($\alpha = -0.1$), and those characteristic of a source dominated by synchrotron radiation (typical value is around $\alpha = -0.8$, Condon 1992, spanning a range as can be seen from Figures 3 and 6). An interesting exception is UM 533, which is the only galaxy detected at all frequencies, with $\alpha_5^{1.4} > 0$. If we consider the galaxies that were not detected at 1.4 GHz we find other 4 sources with spectral slopes in this range (Tol 0619-392, UM 444, Tol 1223-388, and Tol 1358-328). These galaxies are of particular interest for our study, because these spectral indices suggest that these sources are free-free absorbed, and may be related to heavily embedded sources in the early stages of evolution.

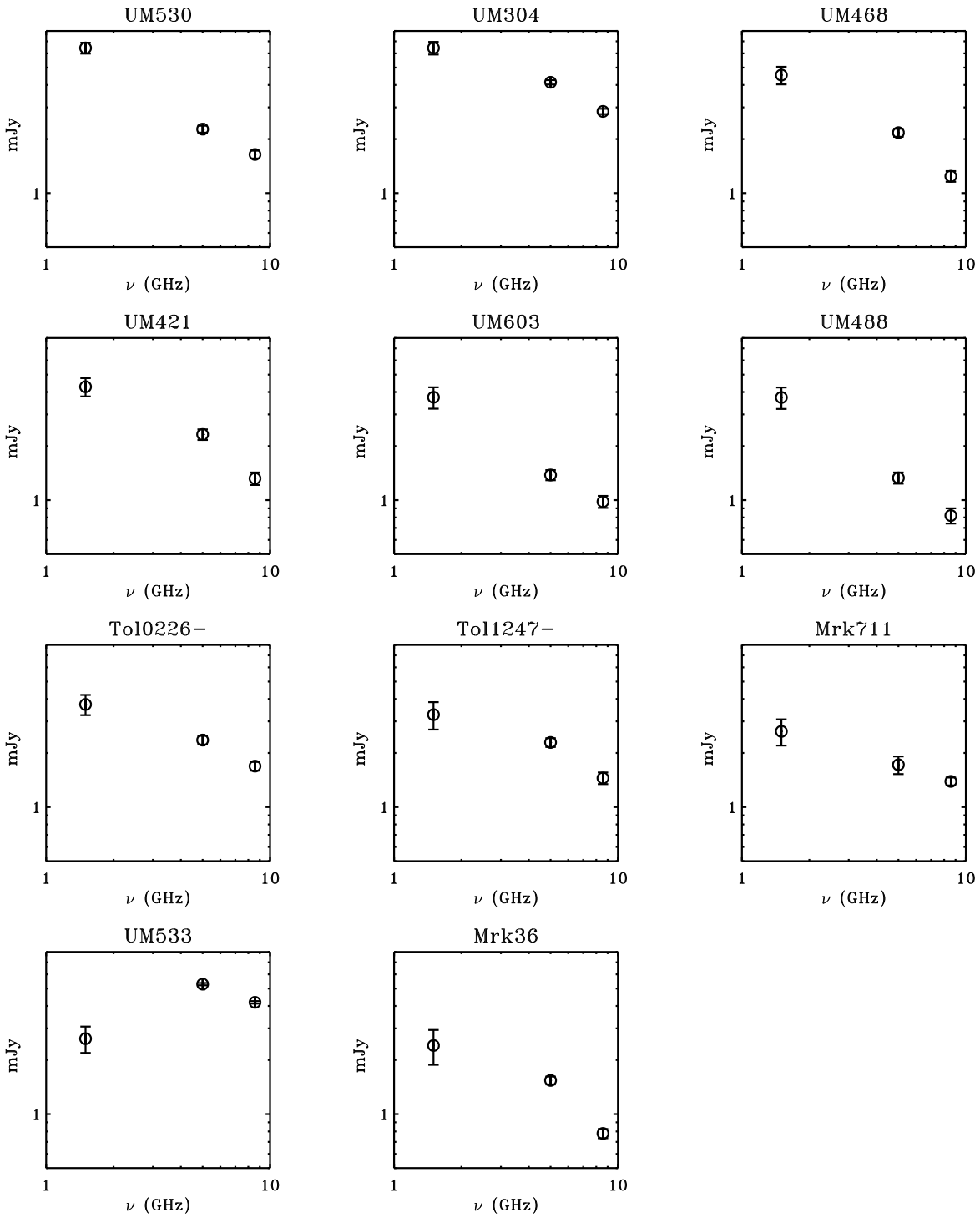

Fig. 1.— Radio SEDs of galaxies detected at all frequencies.

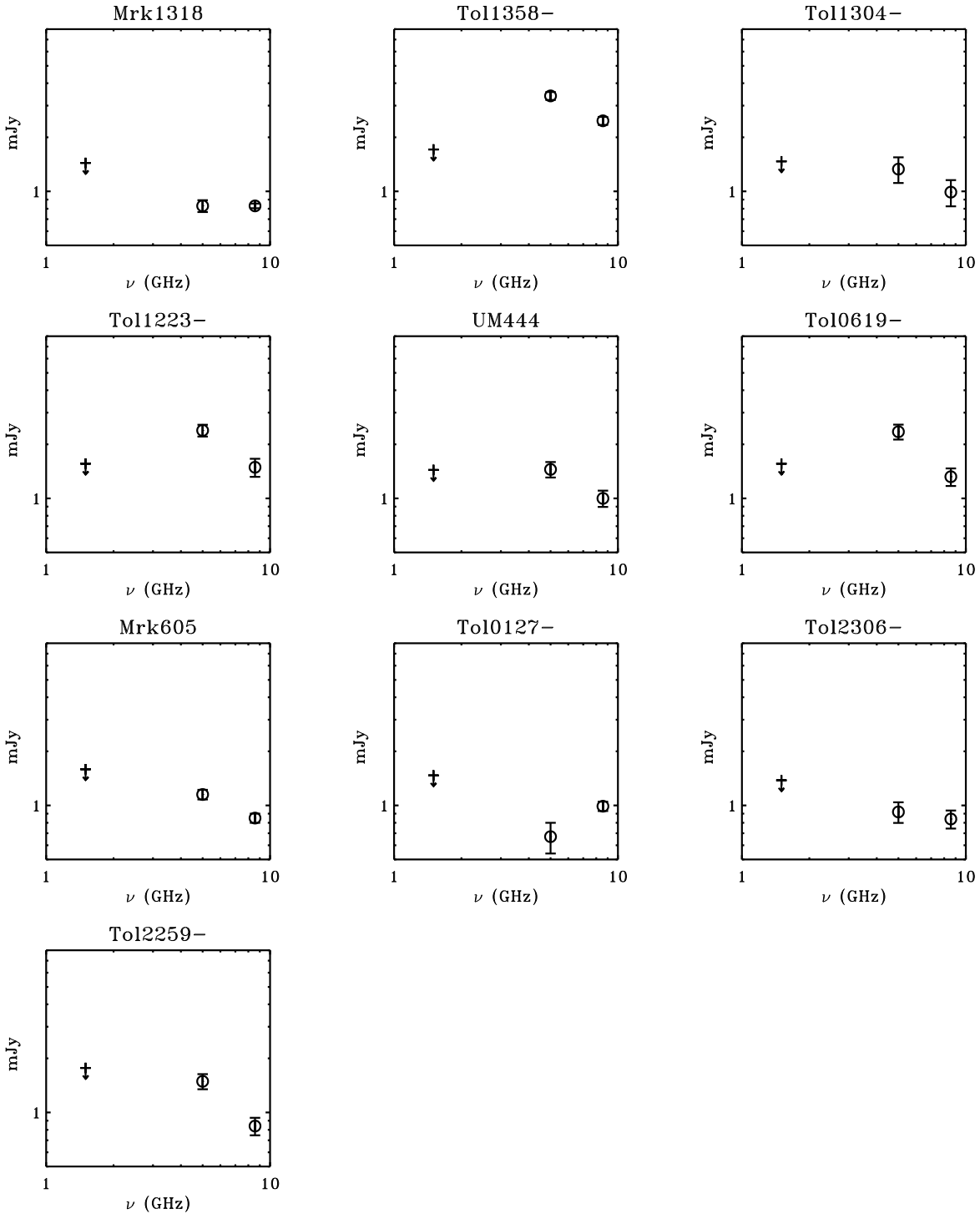

Fig. 2.— Same as Figure 1, but for galaxies not detected at 20 cm. The upper limits at 1.4 GHz correspond to the 3σ value.

In Figure 3 we present the distribution of our galaxies in the F(1.4 GHz) *vs.* F(8.4 GHz) diagram. This Figure also presents two lines indicating the location of thermal ($\alpha = -0.1$) and synchrotron emission ($\alpha = -0.8$). In the case of more evolved star forming galaxies, where we find a mixture of these two components, the 1.4 GHz emission is dominated by synchrotron emission, while at 8.4 GHz both synchrotron and thermal emission have similar contributions. Most of the galaxies in our sample lie in the region between these two lines, indicating that they are young objects still dominated by thermal emission. The position of UM 533 in this diagram (2.6;4.2), as well as other galaxies for which we only have upper limits at 1.4 GHz, is consistent with the description given above.

It is obvious that Figure 3 represents an oversimplification, as the history of star formation is much more complicated and cannot be represented by either continuous or a single burst or even a couple of them (e.g. Terlevich et al. 2004). Keeping this in mind we overplot two qualitative evolutionary tracks to the points in Figure 3. In the first case (solid thick line) we assumed that the galaxies start with only thermal emission from the OB associations, which are heavily absorbed at both 1.4 GHz and 8.4 GHz and can only be detected at the highest frequencies. In this phase the dense giant HII regions are characterized by optically thick free-free emission, which is observed as an inverted spectrum (thermal) radio source and it is commonly named ultradense HII region (Kobulnicky & Johnson 1999, Johnson et al. 2003).

Due to the effect of stellar winds, with typical velocities of 10^3 km s^{-1} and mass losses of about 3 $\times 10^{-5}$M$_\odot$ year^{-1} (e.g. Tenorio-Tagle et al. 1990), the absorbing material starts to blow away, the optical depth is reduced and the galaxy moves in this diagram towards the direction of UM 533 (2.6;4.2). Once all the absorbing material is blown away, the galaxy moves up in this diagram, until it reaches the line where the radio emission is dominated by thermal radiation. As the galaxy continues to evolve, SNe explode, producing copious amounts of synchrotron radiation and moving the galaxies to the top right portion of this diagram where the relation between radio and FIR is obtained (Yun, Reddy & Condon 2001). In this scenario we expect young galaxies to have $\alpha > -0.1$, with the younger objects having the larger slopes due to free-free absorption, evolving towards $\alpha = -0.8$.

In the second scenario we start with some synchrotron emission due to a previous generation of supernovae. If a new burst occurs a new generation of stars is produced, increasing the amount of ionizing photons, and moving the galaxy to the right towards the thermal relation (see dashed thick line in Figure 3). When the next generation of supernova explodes the galaxy starts to move up and right to the position of the non-thermal relation (dot-dashed line). In the next section we explore further these two scenarios by including the analysis of optical data from HIIG91.

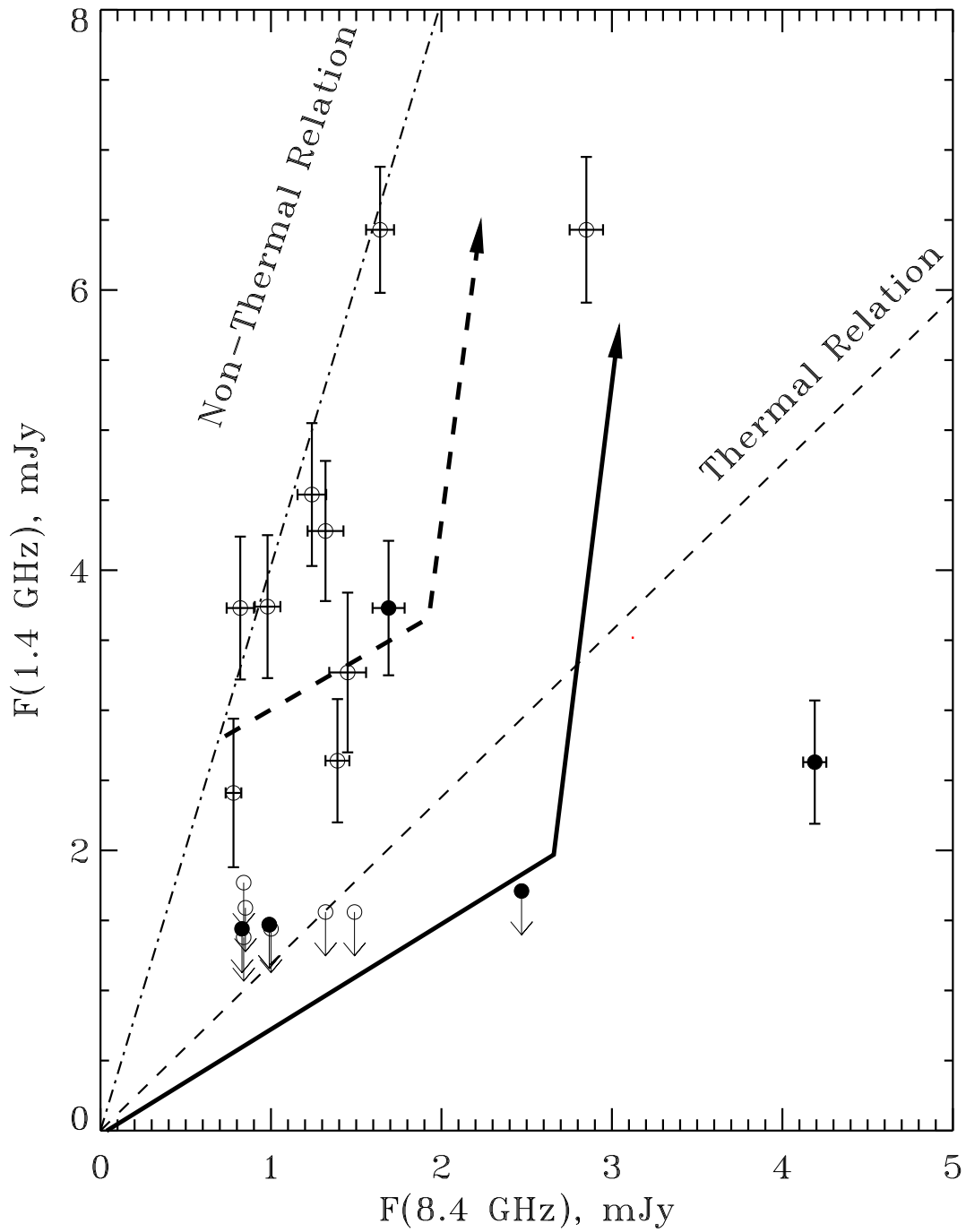

Fig. 3.— Distribution of F(1.4 GHz) as a function of F(8.4 GHz) for the galaxies in Table 2. The dashed thin line shows the expected position of galaxies dominated by thermal emission, while the dot-dashed line shows where galaxies dominated by non-thermal emission are located. Superimposed on this plot are solid-thick and dashed-thick lines indicating qualitative evolutionary tracks described in the text.

5. Optical Properties of the Sample

For the observed galaxies we collected optical spectral information from HIIG91. We corrected by extinction the fluxes of the Hα and Hβ lines using the Milky Way extinction curve (Seaton 1979). The ratios between the observed [OIII]λ5007 and Hβ and the EW(Hβ) are also included in the analysis (Table 3).

The EW(Hβ) has long been used to estimate the age of a stellar burst (e.g. Dottori 1981, Luridiana & Peimbert 2001). However, the EW(Hβ) indicator which consists of the relation between the continuum flux which depends on the whole star formation history of the galaxy and the strength of the emission line which depends on the recent ($\sim 5 \times 10^6$ years) star formation activity can be significantly lower than the age of the current burst. This problem has been noticed in the analysis of the most extreme HII galaxies by Terlevich et al. (2004). To illustrate this problem, we plot in Figure 4 the evolution of the EW(Hβ) for the case of an instantaneous burst and for the case of continuous star formation. Both models were calculated using the SB99 code (Leitherer et al. 1999) for the case of a Salpeter initial mass function and masses between 0.1 and 100M$_\odot$. In both modes the EW(Hβ) decreases with time but due to the formation of new massive stars in the continuous mode, the EW(Hβ) remains larger as time increases. These star forming histories mark the two extrema and the age of a galaxy with a given EW(Hβ) must lie between the limits shown in figure 4. In the case of the existence of an old population, the observed EW(Hβ) is reduced even more – in comparison with the continuous case – due to the integrated light of the galaxy and the absence of massive stars responsible for the recombination lines.

For our sample we found that there is a good correlation between the EW(Hβ) and the strength of the [OIII]λ5007 line which is stronger in the early phases of the starburst when the EW(Hβ) is higher. In fact figure 5 shows that the scatter is higher for those galaxies with EW(Hβ) lower than about 40Å. This figure supports the idea that we are mostly dealing with single young bursts on the upper right corner of the plot, while the bottom left represents a superposition of bursts on an older underlying system.

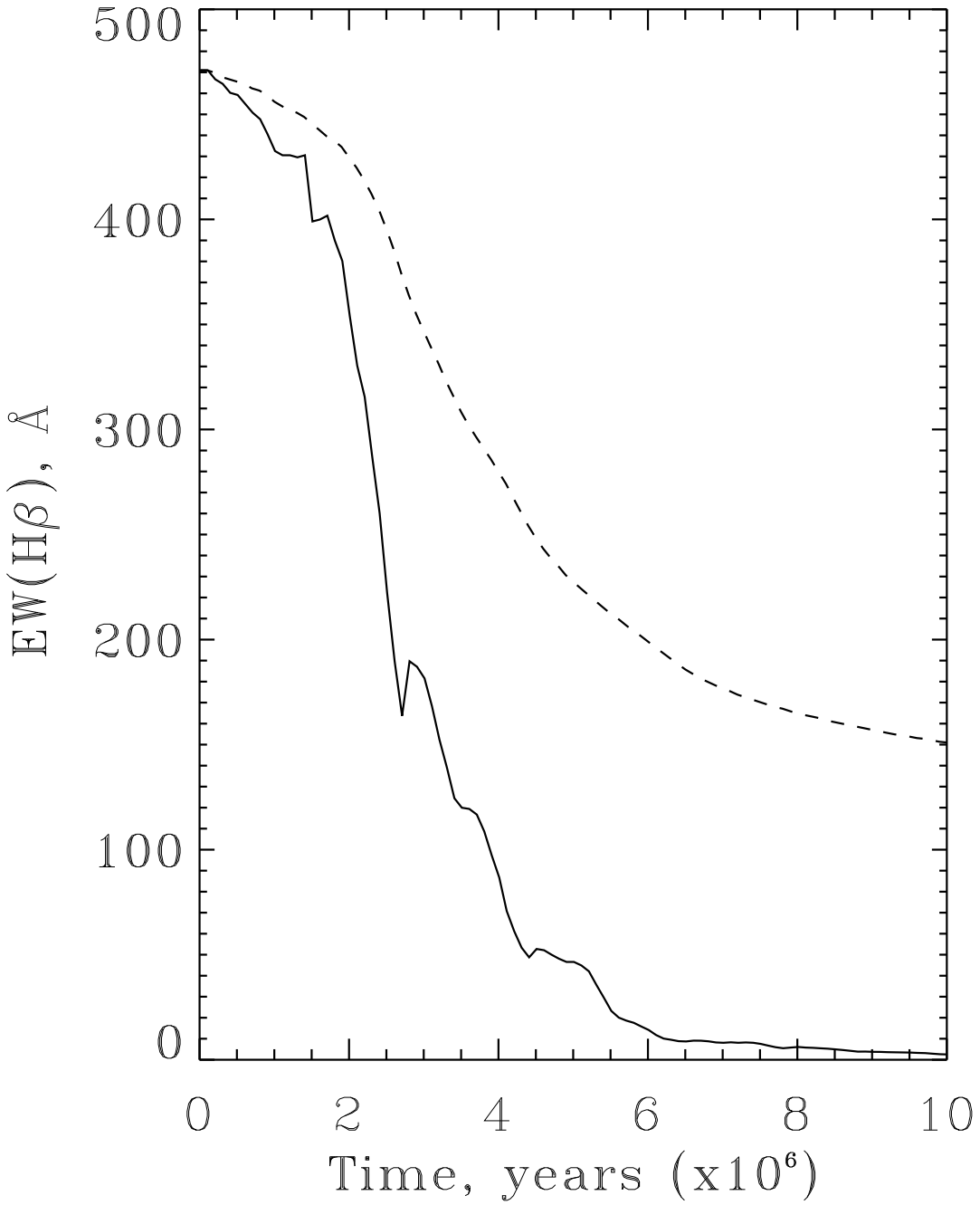

Fig. 4.— Evolution of the EW(Hβ) for the case of an instantaneous burst, solid line, and continuous star formation, dashed line (see text).

Based on the reddening corrected Hα fluxes of the galaxies in the HIIG91 catalog, we estimate their Star Formation Rates (SFR) using the relation given by Rosa-González, Terlevich & Terlevich (2002),

$$\mathrm{SFR}[\mathrm{M}_\odot \mathrm{year}^{-1}] = 1.1 \times 10^{-41} \times \mathrm{L}(\mathrm{H}\alpha) \quad (1)$$

where the L(Hα) is given in erg s^{-1} and must have been corrected by extinction. The relation given by Equation 1 was the result of comparing different indicators of SFR in a well defined sample of starburst galaxies and using as reference the SFR given by the FIR. The conversion between Hα luminosities and SFR is in any case just 15% higher than the conversion given by other authors (e.g. Kennicutt, Tamblyn & Condon 1994; Madau, Pozzetti & Dickinson 1998). The extinction corrected values of the Hα and Hβ fluxes together with the corresponding SFRs are given in Table 3.

We make use of the SB99 code to estimate the mass of the current burst. In the case of an instantaneous burst, a stellar cluster of 10^6 M$_\odot$ produces a luminosity in Hα of about 3.2×10^{40} erg s^{-1}. The obtained luminosities and derived masses are given in Table 3.

6. Combining Optical and Radio Measurements

In this section we combine the radio and optical data described in previous sections in order to test the evolutionary models outlined in section 4.

After an episode of star formation, the first SN explosion and consequently the first contribution to the synchrotron emission appears at about 3.5×10^6 years, which corresponds to an EW(Hβ) of about 120 Å for the case of an instantaneous burst or 310 Å in the case of continuous star formation (Figure 4). Therefore objects with high EW(Hβ) and flat slopes are candidates to be galaxies dominated by very recent starburst episodes.

Figure 6 shows the relation between the EW(Hβ) and the $\alpha_5^{1.4}$ where objects with EW(Hβ) $>$ 100Å have slopes higher than -0.5. A similar relation is found for the case of $\alpha_5^{1.4}$ and the ratio [OIII]λ5007/Hβ. In fact all the galaxies with EW(Hβ) $>$ 40Å and [OIII]λ5007/H$\beta \gtrsim$ 4 are flatter than $\alpha_5^{1.4} > -0.5$ (figure 5). Although Figure 6 is a scattered plot, there is a tendency marked by the fact that the points distribution is different in both sides of the vertical line corresponding to the separation between "young-simple" and "old-complex" systems (Figure 5).

For the galaxies with lower EW(Hβ) and detected at 20 cm there is a weak trend where galaxies with lower EW(Hβ) have lower values for the spectral index $\alpha_5^{1.4}$. Deeper VLA observations of galaxies not detected at 20 cm but with EW(Hβ) $\gtrsim$ 5 (age of about

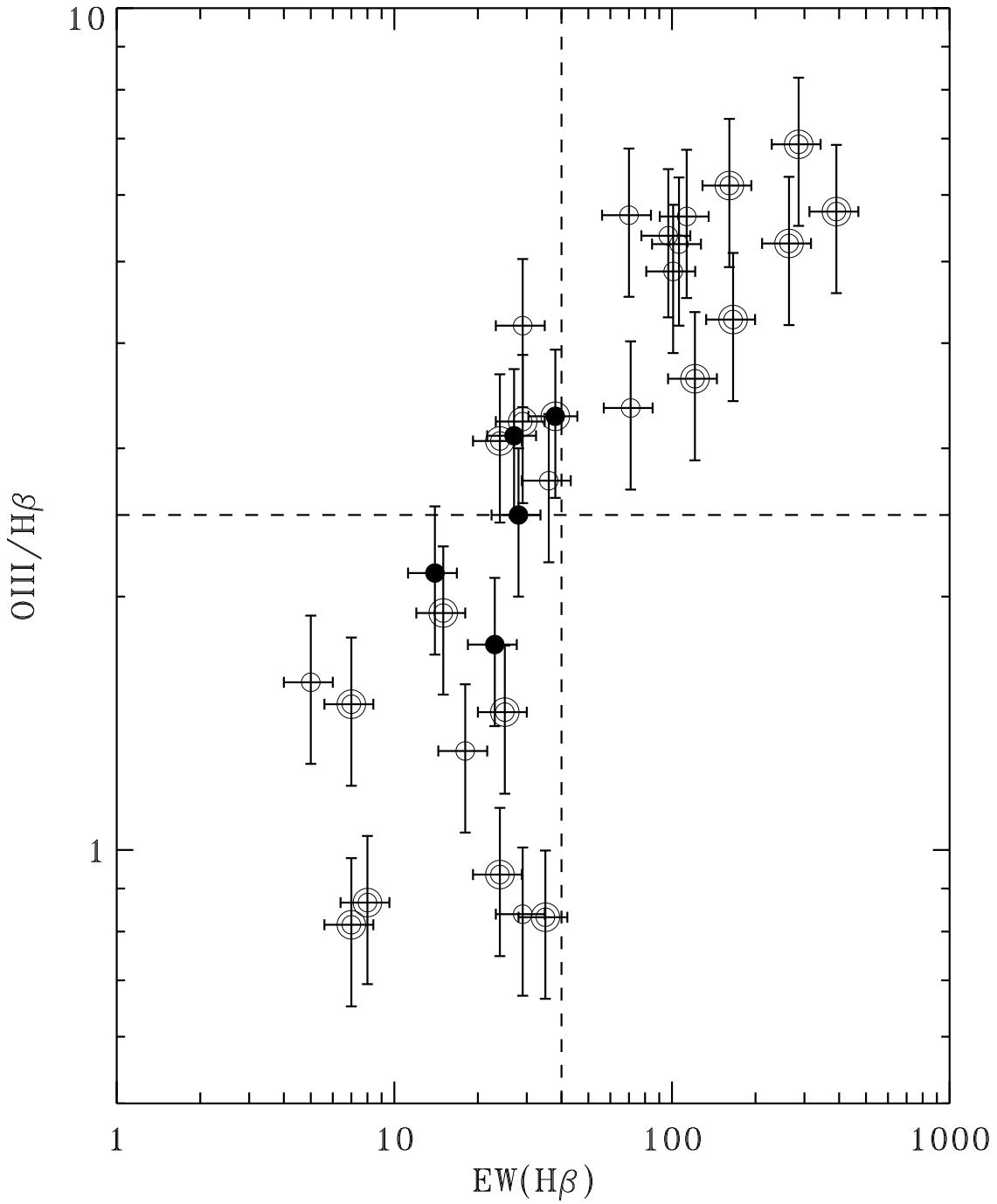

Fig. 5.— Correlation between the EW(Hβ) and the ratio OIII/Hβ. Galaxies with $\alpha_5^{1.4} < -0.5$ (solid circles) and with $\alpha_5^{1.4} \geq -0.5$ (open symbols) are represented. Double circles indicate those galaxies for which the 20 cm flux is just an upper limit. The vertical dashed line is at EW(Hβ)=40Å and separates two regions of the plot with different scatter; the horizontal dashed line separates regions of low from high excitation (see description in the text).

8×10^6years for an instantaneous burst) will be obtained in the near future. Massive stars within a young burst ionize the surrounding media producing free electrons and the presence of recombination lines. The intensity of the Hβ emission line is related to the free-free radiation observed at radio wavelengths by (Condon 1991),

$$\mathrm{H}\beta\,(\mathrm{erg\,s^{-1}cm^{-2}}) = 2.8\times10^{-11}(\mathrm{Te}/10^4)^{-0.52}\nu^{0.1}\mathrm{F}_\nu \quad (2)$$

where Te is the electron temperature of the plasma, ν is the frequency of the observation (expressed in GHz) and F_ν is the flux in mJy at the given frequency.

For a normal galaxy (normal in the sense that it follows Yun et al. 2001) dominated by synchrotron radiation, the thermal emission is about 10 percent of the synchrotron radiation at 1.4GHz. However, due to the different behavior and slopes of thermal and non-thermal emission, the thermal emission at 8.4GHz (3.5cm) could be about 50 percent of the synchrotron one or even more for those galaxies that are synchrotron deficient (Condon 1992; Schmitt et al. 2006). Figure 7 (top panel) shows the extinction corrected Hβ flux against the flux at 8.4GHz. Most of the galaxies have fluxes which are consistent with thermal emission from plasmas with temperatures between 10^4K (solid line) and 5×10^4K (dashed line). However some galaxies have an excess of radio emission due to the presence of synchrotron emission.

At 20 cm (1.4GHz: bottom panel in Figure 7) the flux is clearly contaminated by the presence of synchrotron emission. As in the top panel the solid and dashed lines represent the thermal emission based on Equation 2. All the galaxies detected at 20 cm have fluxes above the thermal limits, however the galaxies not detected at 20 cm (the upper limits) are close to the thermal region.

Due to the presence of massive stars in normal and starburst galaxies, there is a strong relation between the observed FIR and the flux at 1.4 GHz. This correlation, which covers several orders of magnitude in luminosities, is explained by the presence of massive stars which heat the dust producing the observed FIR radiation and, as a consequence of the short life time of these stars, they explode as SN producing the synchrotron emission observed at 1.4 GHz (Yun et al. 2001). Combining this strong correlation with the relation between the FIR luminosities and the current SFR from Kennicutt (1998), Yun and collaborators proposed a robust relation between the luminosities at 1.4 GHz and the SFR,

$$\mathrm{SFR}[\mathrm{M_\odot year^{-1}}] = 5.9\times10^{-29}\times\mathrm{L_{1.4GHz}} \quad (3)$$

where the luminosities are expressed in units of erg $\mathrm{s^{-1}}$ $\mathrm{Hz^{-1}}$. Schmitt et al. (2006) found a similar relation using a slightly different approach. Notice that all SFR estimates have

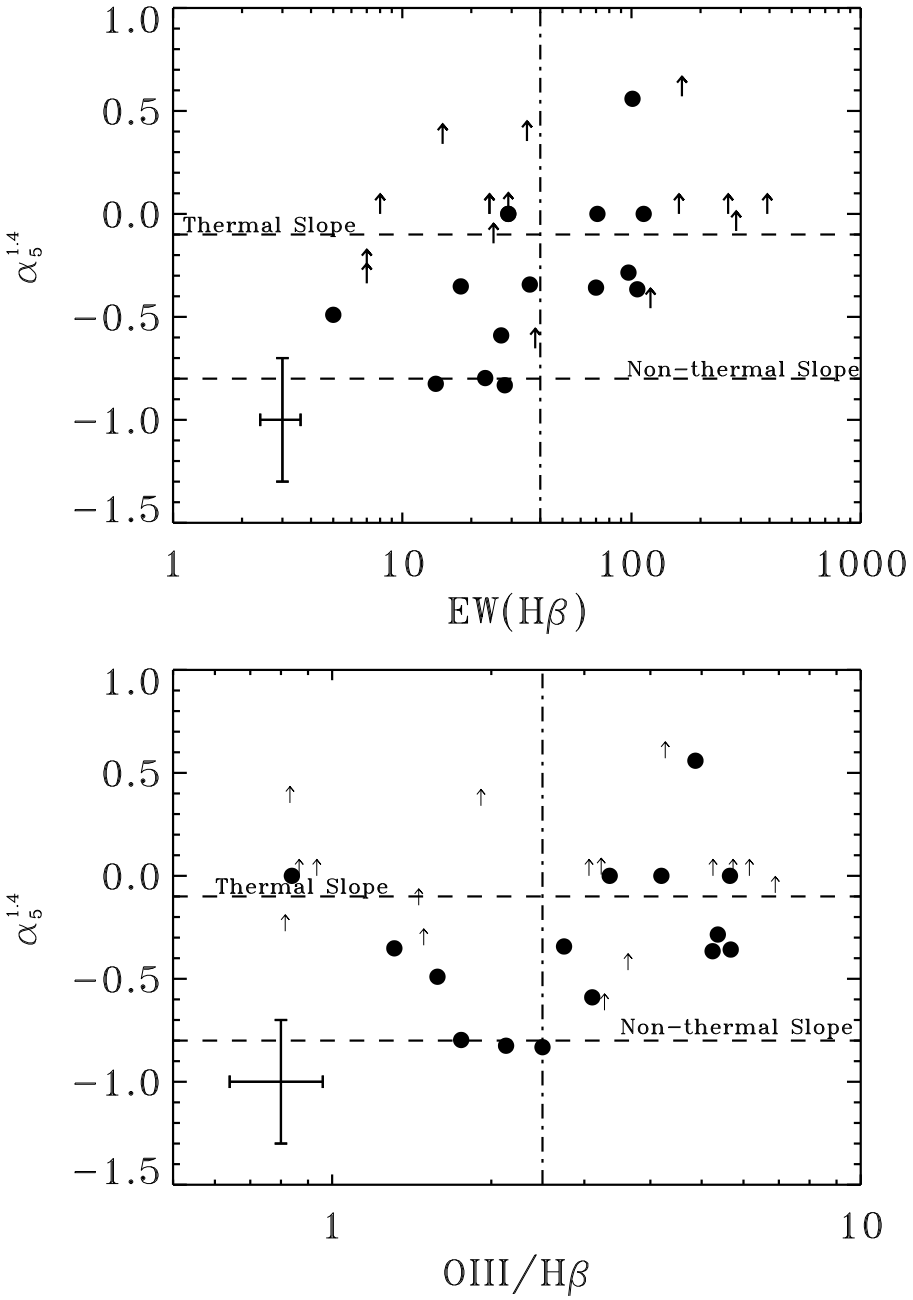

Fig. 6.— Variation of the spectral index ($\alpha_5^{1.4}$) with respect to the EW(Hβ) (upper panel) and to the ratio OIII/Hβ (lower panel). In both panels the canonical values for the thermal ($\alpha = -0.1$) and non thermal slopes ($\alpha = -0.8$) are represented by dashed lines. Dot-dashed lines in both panels reproduce the boundaries indicated by the dashed lines in Figure 5.

uncertainties, because each estimator traces different populations and depend on several assumptions, e.g. the initial mass function, or on the light attenuation which is a strong function of wavelength.

Comparing the SFR estimated by the 1.4 GHz luminosities with those given by the recombination lines (Table 3) we find that the optical SFR is on average 4 times higher than the SFR given by the radio luminosities. In the bottom panel of Figure 7 we plot a dot-dashed line where the optical SFR is equal to the radio SFR based on the Yun et al. (2001) relation. Only three galaxies are close to the dot-dashed line showing that most of the observed starbursts still are in the early stages of evolution, when not too many stars have exploded as SN, and as a result the observed radio SED is dominated by thermal emission. The most extreme cases are those galaxies with non detection at 20 cm. The cases with clear signature of free-free absorption and those dominated exclusively by thermal emission are similar to the regions detected by Cannon & Skillman (2004) within NGC 625, and by Johnson & Kobulnicky (2003) in He2-10. Observations with higher angular resolution are necessary to understand the nature of these sources.

The deficit of 1.4GHz emission showed by Figure 7 can be quantified in terms of the ratio between the observed 1.4 GHz flux and the expected flux based on the SFR calculated using the optical emission lines and equation (3). For simplicity we denoted this ratio as the d-parameter. Figure 8 shows the EW(Hβ) against the d-parameter expressed in percentage. Notice that most of our galaxies lie in a region where the observed flux is less than 50% of the expected value, showing that indeed our sample has a deficit of synchrotron radiation. Five galaxies (Tol 116-325, MRK 1315, Tol 1303-281, Tol 1304-386 and Tol 1358-328) are extreme cases with the highest EW(Hβ) and just upper limits in the observed 1.4 GHz fluxes. Notice that, based on the EW(Hβ), these galaxies have ages of less than 10^7 years even in the case of continuous star formation (see Figure 4).

In order to investigate how our galaxies compare to normal, quiescent star forming galaxies in the $d-$parameter $vs.$EW(Hβ) diagram, we obtained radio 1.4 GHz fluxes (from NVSS) for a sample of such galaxies from Ho, Filippenko, & Sargent (1997), and Jansen et al. (2000). For the Ho et al. (1997) sample we obtained integrated Hα fluxes and EW(Hβ) from Moustakas & Kennicutt (2006) (EW(Hβ) was calculated using the emission line and broad band fluxes). For the Jansen et al. (2000) sample these values were obtained from Kewley et al. (2002). The sample, their EW(Hβ)'s, SFR(Hα) corrected for extinction, SFR(1.4 GHz), F(1.4 GHz) and d-parameters are presented in Table 5. We can see in Figure 8 that the normal galaxies have small EW(Hβ) and large d values, occupying a different region relative to the galaxies in our sample, again consistent with the interpretation that our galaxies are young and have a deficit of synchrotron radiation. A particularly interesting result from this

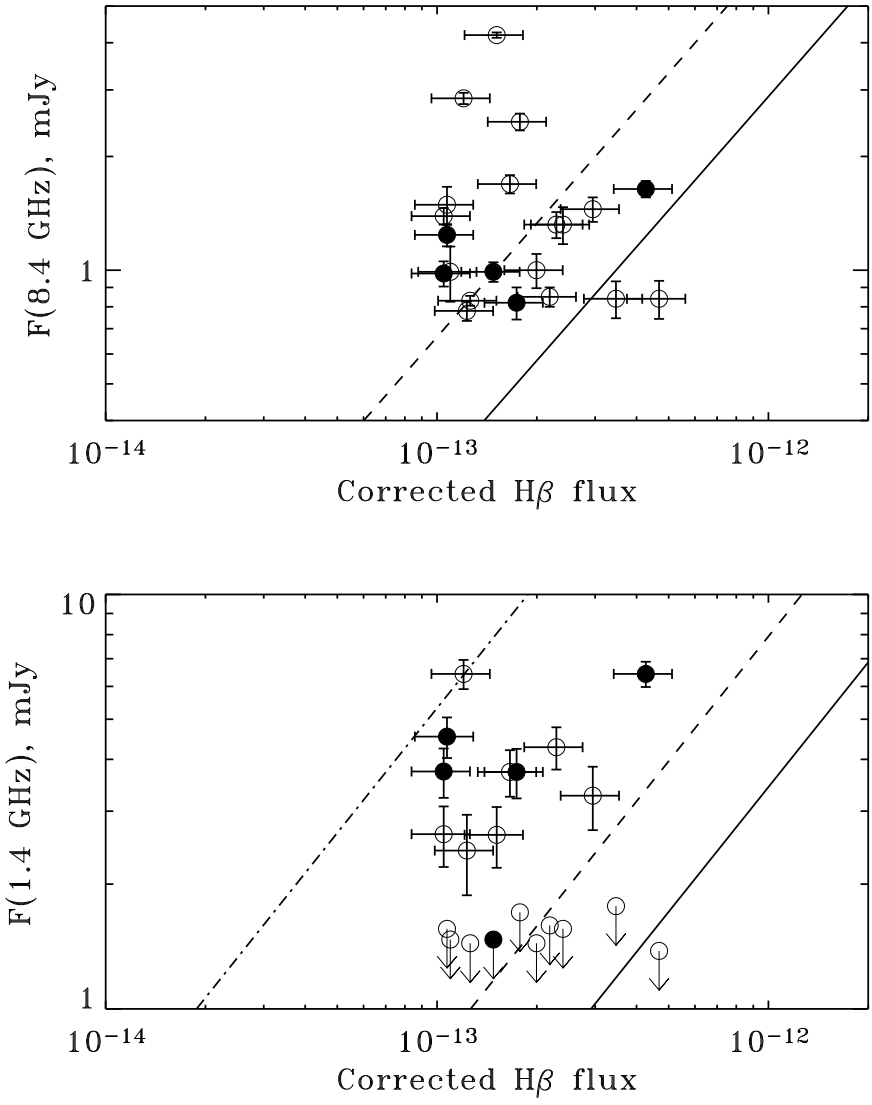

Fig. 7.— Relation between the extinction corrected Hβ flux, the flux at 8.4 GHz (top panel) and the flux at 1.4 GHz (bottom panel). In both panels the solid line is the relation between the strength of the Hβ line and the corresponding radio flux for the case of thermal emission coming from a plasma with a temperature of 10^4K. The dashed lines correspond to a temperature of 5×10^4K. In the bottom panel we draw (dot-dashed-line) the relation given by Yun et al. (2001) which includes synchrotron emission. In both panels, the solid symbols are galaxies with $\alpha_5^{1.4} > -0.5$. Non detections are represented by the arrows (upper limits).

Figure is the fact that a significant portion of the normal galaxies, those with the smaller EW(Hβ)'s, have d>100%. Although this result seems contradictory, since it implies a higher radio SFR than what is observed in Hα, it can be explained in view of the lifetime of these two indicators. For example, in the case of a single burst, the Hα emission lasts only 10 Myr, until all the ionizing photons die. The radio emission on the other hand will last much longer than that, because of the longer synchrotron emission life time and the fact that the stars that explode as SN last for $\sim$40 Myr.

7. The Far Infrared and the q parameter

A fraction of the optical-uv light emitted by young and massive stars is absorbed by dust grains and re-emitted in the far infrared regime making this wavelength range an excellent tracer of the recent star forming activity.

The q parameter is defined as the ratio between the FIR and radio fluxes (Helou, Soifer and Rowan-Robinson 1985),

$$q = log\left(\frac{FIR/3.75\times10^{12}\mathrm{Hz}}{S_{1.4GHz}}\right) \tag{4}$$

to quantify the strong correlation between the radio continuum and the FIR observed in a sample of disk- and starburst- galaxies.

In order to estimate the q parameter of our sample of galaxies we obtained from the IRAS catalog (Moshir et al. 1990) the fluxes at 60 μm (S_{60}) and 100 μm (S_{100}). The FIR flux is calculated using the expression from Young et al. (1989),

$$FIR\,(\,\mathrm{W\,m^{-2}}) = 1.26\times10^{-14}(2.58\times S_{60}+S_{100}) \tag{5}$$

where the fluxes are given in Jy (Table 4). In those cases where the 100 μm flux is just an upper limit we apply a bolometric correction based on multigrain dust models for the FIR emission presented by Rowan-Robinson & Efstathiou (1993). Following this work, the FIR luminosity is about 1.7 times the luminosity at 60 μm (see also Rowan-Robinson et al. 1997, Chapman et al. 2000 for the application of this bolometric correction to a different set of starforming galaxies).

Figure 9 indicates a trend between the q parameter and the radio spectral index $\alpha_5^{1.4}$. This figure shows that galaxies with a $q \lesssim 2.35$ – the canonical value of the q parameter (Helou et al. 1985, Roussel et al. 2003) – are located closer to the synchrotron slope confirming the relation observed in large samples of normal and starburst galaxies (e.g. Yun et al. 2001).

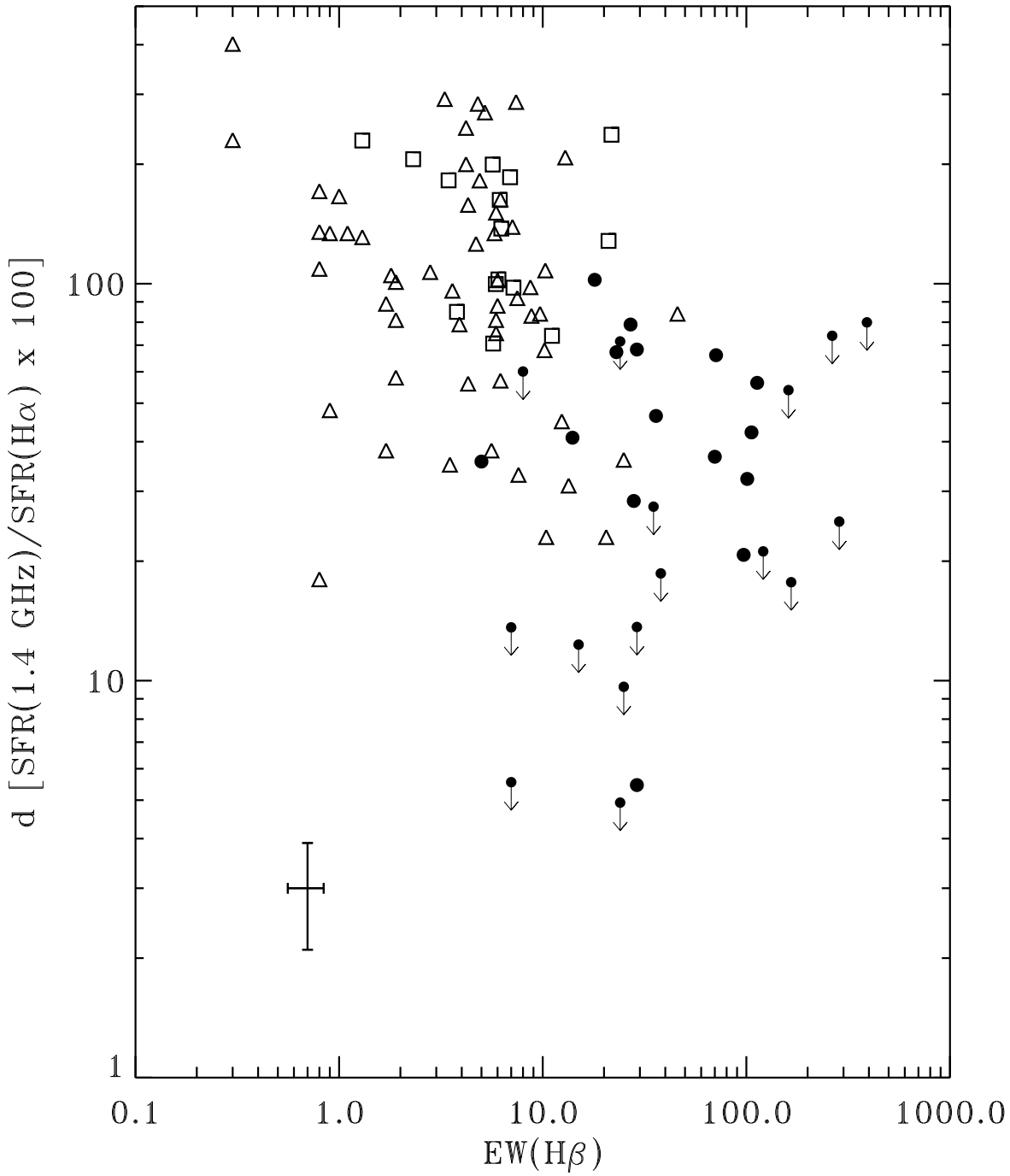

Fig. 8.— Hβ equivalent width against the d parameter defined as the ratio between the observed and the expected 1.4 GHz flux (see text for further details). Circles are the sample HII galaxies and open symbols represent the control sample from Jansen et al. (2000) (triangles) and from Ho et al. (1997) (squares).

However galaxies with high q parameter are in general close to- or above the line defined by the thermal radio emission slope. In some extreme cases the q parameter is higher than 2.75. Such extreme galaxies have been reported in the literature (e.g. NGC 1377, NGC 4491, NGC 4418, Roussel et al. 2003). A high value of the q parameter and a positive radio spectral index point to the presence of free-free absorption as has been observed in very young systems (Tarchi et al. 2000, Vacca, Johnson & Conti 2002, Johnson & Kobulnicky 2003).

In order to compare our results with a large sample of galaxies, we analyzed the distribution of HII galaxies from Ho, Filippenko & Sargent (1997) in the q vs. $\alpha_5^{1.4}$ plot. These galaxies span a wide range of characteristics, from sources similar to the ones studied in this paper to quiescent star forming galaxies. Table 6 presents the galaxies from Ho et al. (1997) for which we could find integrated 1.4 GHz, 4.9 GHz and IRAS fluxes in the literature. The 1.4 GHz fluxes were obtained from NVSS, requiring the addition of multiple components in the case of the most extended sources. For the 4.9 GHz we used data from single dish observations, mostly from Gregory & Condon (1991), which had a resolution comparable to that of NVSS. Using Equation 4 we estimate the q parameter and plot these results with our galaxies in Figure 9. As expected, based on previous studies of normal galaxies (e.g. Condon 1992), most of the galaxies lie in a region characterized by a q parameter around 2.5, and synchrotron like slope ($\alpha_5^{1.4} \lesssim -0.5$). Only NGC 4214 has characteristics of a young galaxy and it is located close to NGC 5253. Notice also that, when the Ho et al. (1997) galaxies are included in this plot, a much clearer trend emerges. Galaxies with large q parameters tend to have large $\alpha_5^{1.4}$ slopes, strengthening the idea that they are young sources in the early stages of evolution. Conversely sources with lower q values usually have smaller $\alpha_5^{1.4}$ slopes, indicating that they are at a much more advanced evolutionary stage.

8. Discussion and Conclusions

The tight correlation between far infrared (FIR) and radio luminosity confirms that radio emission is also a good tracer of recent star formation (Yun et al. 2001). The origin of this correlation is the population of massive stars that are responsible for the dust heating, the FIR radiation and the supernova activity that generates the radio emission.

However, deviations from this correlation are expected both in the early phases of a starburst – before the first Type II SNe explode – or in the post-starburst phase when the synchrotron emission ages and is also contaminated by the emission from less massive stars (Bressan et al. 2002).

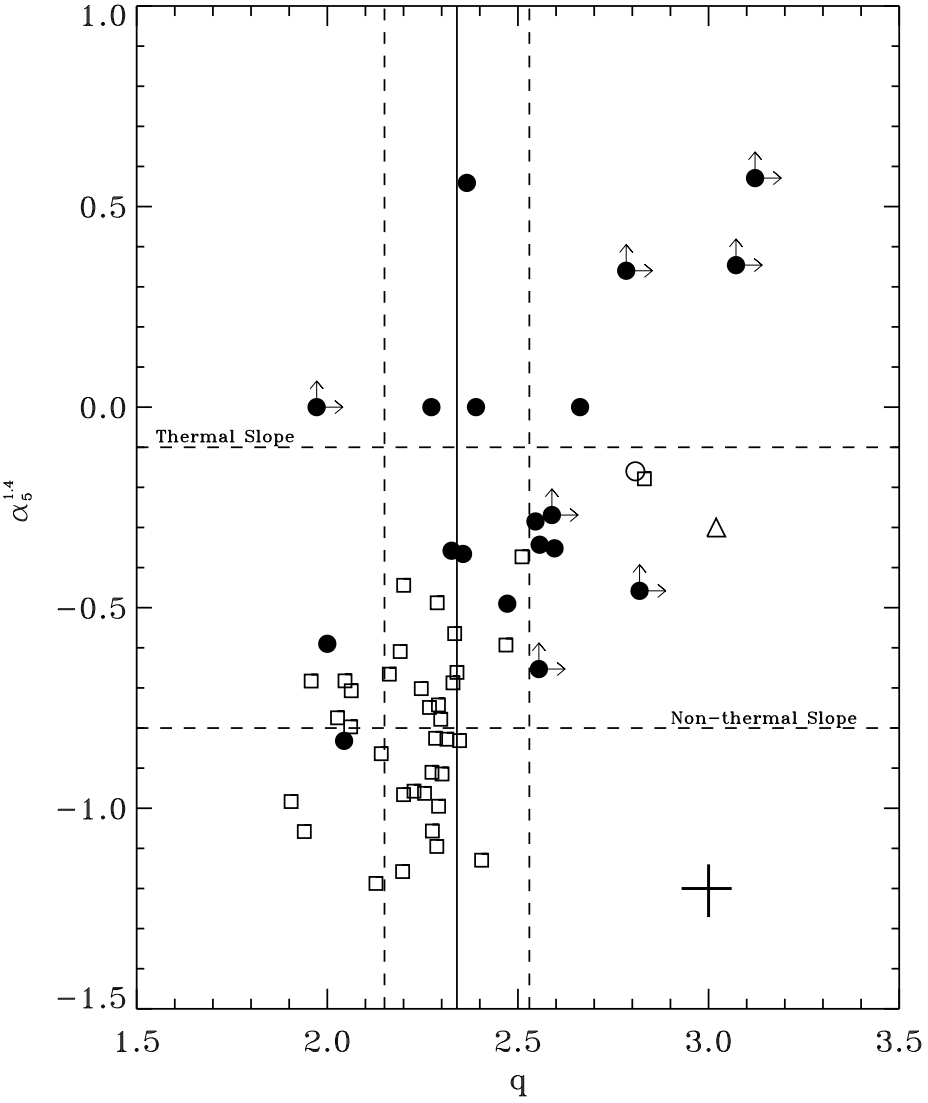

Fig. 9.— Estimated q parameter for the galaxy sample plotted against the radio spectral index between 1.4 and 5 GHz (solid circles). The solid line shows the value of q found by Roussel et al. (2003). Two vertical dashed lines show the one sigma error of this determination. Two well studied *nascent* galaxies are plotted, NGC 5253 (open circle, Turner et al. 1998) and NGC 4418 (triangle, Roussel et al. 2003). The squares correspond to a sample of normal galaxies extracted from Ho et al. (1997). The horizontal dashed lines show the theoretical values of the slope for the cases of thermal and non-thermal emission. The cross at the bottom right corner represents a typical error bar of mean uncertainties of about 15% for both IRAS and radio data.

Based on the combination of optical, FIR and radio data, we have detected a large deviation from the FIR-radio correlation within a sample of normal and starburst galaxies. Our sample of 31 galaxies is strongly biased to young systems which have strong EW(Hβ) and relatively high SFR. Only a few galaxies in our sample follow the Yun et al. (2001) relation and the SFR calculated from radio continuum at 1.4 GHz is a factor of 4 below the SFR given by optical emission lines. We quantified this deficit introducing the d-parameter which is the ratio between the observed radio continuum flux at 1.4 GHz and the expected one calculated using the SFR provided by the optical emission lines (Hα) and the empirical relation given by Yun et al. (2001) which relates the flux at 1.4GHz with the current SFR determined by the FIR emission. In most of the cases the d-parameter is well below 50% with only 2 galaxies having values above 75%.

The summary of our results is presented in Table 7. We tabulated the extreme values of the parameters which point to the existence of a recent star forming event in our sample of galaxies. The indicators with high values of the EW(Hβ) and [OIII]λ5007/Hβ ratio, have a value of $\alpha_5^{1.4}$ typical of a region dominated by thermal emission, a low d parameter, and a high q parameter. Only two galaxies, Mrk 1318 and Tol 1358-328 have the five indicators corresponding to very young objects while 5 galaxies present 4 of the 5 indicators. In the galaxies Tol 0226-390, Tol 1247-232 and UM 533 the only indicator not pointing to a very young system is the q parameter which is in all cases very close to the canonical value. For the case of Tol 1304-386 we have no FIR information so we could not estimate the q parameter. Mrk 711 has a relatively low EW(Hβ) but a high [OIII]λ5007/Hβ ratio, pointing to the existence of a new burst on top of an older stellar population. In this galaxy all the other tracers of a young population are present. Another 10 galaxies show signs of young systems in 3 of the 5 tracers considered (see Table 7) and are also extremely good candidates to look for deeply embedded super stellar clusters where only thermal radio and mid infrared radiation can be detected.

For the early phase deviation to occur, a highly synchronized star formation is required, i.e. the massive star forming phase should be shorter than ∼3-4Myr in order to prevent the appearance of the first supernovae associated to the more massive stars and the consequent synchrotron emission. This also suggests that there has been no large starforming event in the previous 10^8yr. The results summarized above have important implications not only for low mass galaxy evolution but also for the study of young massive star clusters and for the understanding of the early stages of their evolution. We showed that by combining optical spectroscopy with radio continuum observations we can efficiently detect extremely young systems, before the first Type II SNe explode. These systems represent a significant enlargement of the current sample of nearby starbursts, like Henize 2-10 (Johnson & Kobulnicky 2003) and NGC 5253 (Beck et al. 1996, Turner et al. 2000, Turner & Beck 2004), known to

have these properties. A detailed higher resolution study of these sources, to be published in a forthcoming paper, will be extremely valuable for the understanding of their properties and to study evolutionary scenarios. Furthermore, we hope that the study of a complete sample will allow the segregation between instantaneous and extended starformation scenarios.

The National Radio Astronomy Observatory is a facility of the National Science Foundation, operated under cooperative agreement by Associated Universities, Inc. This research made use of the NASA/IPAC Extragalactic Database (NED), which is operated by the Jet Propulsion Laboratory, Caltech, under contract with NASA. Basic research at the US Naval Research Laboratory is supported by the Office of Naval Research.

Computer facilities for DRG were kindly provided by *Dos-Informática*, Tenerife. RT and ET acknowledge support by the Mexican research council (CONACYT) under grant 40018. HRS thanks the hospitality of INAOE for a visit during a Guillermo Haro Advanced Program in Astrophysics workshop when this project was conceived. The authors are very grateful to an anonymous referee whose comments and suggestions largely improved this manuscript.

REFERENCES

Beck, S. C., Turner, J. L., Ho, P. T. P., Lacy, J. H., & Kelly, D. M. 1996, ApJ, 457, 610

Becker, R. H., White, R. L., & Edwards, A. L. 1991, ApJS, 75, 1

Bressan, A., Silva, L., & Granato, G. L. 2002, A&A, 392, 377

Cannon, J. M., & Skillman, E. D. 2004, ApJ, 610, 772

Chapman, S. C., et al. 2000, MNRAS, 319, 318

Condon, J. J. 1992, ARA&A, 30, 575

Condon, J. J., Anderson, E., & Broderick, J. J. 1995, AJ, 109, 2318

Dottori, H. A. 1981, Ap&SS, 80, 267

Gregory, P. C., & Condon, J. J. 1991, ApJS, 75, 1011

Griffith, M. R., Wright, A. E., Burke, B. F., & Ekers, R. D. 1995, ApJS, 97, 347

Helou, G., Soifer, B. T., & Rowan-Robinson, M. 1985, ApJ, 298, L7

Ho, L. C., Filippenko, A. V., & Sargent, W. L. W. 1997, ApJ, 487, 579

Hoyos, C., & Díaz, A.I. 2006, MNRAS, 365, 454

Jansen, R. A., Fabricant, D., Franx, M., & Caldwell, N. 2000, ApJS, 126, 331

Johnson, K. E., Kobulnicky, H. A., Massey, P., & Conti, P. S. 2001, ApJ, 559, 864

Johnson, K. E., Indebetouw, R., & Pisano, D. J. 2003, AJ, 126, 101

Johnson, K. E., & Kobulnicky, H. A. 2003, ApJ, 597, 923

Johnson, K. E. 2004, New Astronomy Review, 48, 1337

Kennicutt, R. C. 1998, ARA&A, 36, 189

Kennicutt, R. C., Tamblyn, P., & Congdon, C. E. 1994, ApJ, 435, 22

Kewley, L. J., Geller, M. J., Jansen, R. A., & Dopita, M. A. 2002, AJ, 124, 3135

Kobulnicky, H. A., & Johnson, K. E. 1999, ApJ, 527, 154

Leitherer, C., et al. 1999, ApJS, 123, 3

Luridiana, V., & Peimbert, M. 2001, ApJ, 553, 633

Madau, P., Pozzetti, L., & Dickinson, M. 1998, ApJ, 498, 106

Moustakas, J., & Kennicutt, Jr., R. C. 2006, ApJS, 164, 81

Moshir, M., et al. 1990, BAAS, 22, 1325

Raimann, D., Bica, E., Storchi-Bergmann, T., Melnick, J., Schmitt, H. 2000a, MNRAS, 314, 295

Raimann, D., Bica, E., Storchi-Bergmann, T., Melnick, J., Schmitt, H. 2000b, MNRAS, 316, 559

Rosa-González, D., Terlevich, E., & Terlevich, R. 2002, MNRAS, 332, 283

Roussel, H., Helou, G., Beck, R., Condon, J. J., Bosma, A., Matthews, K., & Jarrett, T. H. 2003, ApJ, 593, 733

Rowan-Robinson, M., & Efstathiou, A. 1993, MNRAS, 263, 675

Rowan-Robinson, M., et al. 1997, MNRAS, 289, 490

Seaton, M. J. 1979, MNRAS, 187, 73

Schmitt H. R., Calzetti D., Armus L., Giavalisco M., Heckman T. M., Kennicutt R. C., Jr., Leitherer C., Meurer G. R., 2006, ApJ, 643, 173

Skillman, E.D., Terlevich, E., & Terlevich, R. 1998, Space Science Reviews 84, 105-114. Kluwer Academic Publishers, Belgium.

Tarchi, A., Neininger, N., Greve, A., Klein, U., Garrington, S. T., Muxlow, T. W. B., Pedlar, A., & Glendenning, B. E. 2000, A&A, 358, 95

Telles, E., & Terlevich, R. 1997 MNRAS, 286, 183

Tenorio-Tagle, G., Bodenheimer, P., Franco, J., & Rozyczka, M. 1990, MNRAS, 244, 563

Terlevich, R., Melnick, J., Masegosa, J., Moles, M., & Copetti, M. V. F. 1991, A&AS, 91, 285 (HIIG91)

Terlevich, R., Silich, S., Rosa-González, D., & Terlevich, E. 2004, MNRAS, 348, 1191

Turner, J. L., Ho, P. T. P., & Beck, S. C. 1998, AJ, 116, 1212

Turner, J. L., Beck, S. C., & Ho, P. T. P. 2000, ApJ, 532, L109

Turner, J. L., & Beck, S. C. 2004, ApJ, 602, L85

Vacca, W. D., Johnson, K. E., & Conti, P. S. 2002, AJ, 123, 772

Young, J. S., Xie, S., Kenney, J. D. P., & Rice, W. L. 1989, ApJS, 70, 699

Yun, M. S., Reddy, N. A., & Condon, J. J. 2001, ApJ, 554, 803

Table 1. Sample and Image Reconstruction Parameters

Name	RA	DEC	V_{Rad}	1.4 GHz		4.9 GHz		8.4 GHz		
	(J2000.0)		(km s^{-1})	$b_{maj} \times b_{min}$ ($''$)	PA (°)	$b_{maj} \times b_{min}$ ($''$)	PA (°)	$b_{maj} \times b_{min}$ ($''$)	PA (°)	Program[a]
UM 304	01 06 54.1	+01 56 44	4708	54.1×47.5	40.8	18.3×14.6	54.4	10.3×8.5	61.2	AG674
Tol 0127-397	01 29 15.9	-39 30 38	4797	50.4×45.4	30.7	43.0×12.6	6.5	2.8×0.6	-8.1	AG674,AS734
Tol 0145-391	01 47 10.3	-38 52 53	16250	54.4×47.1	-24.2	40.8×12.7	6.7	24.1×7.4	11.4	AG674
Tol 0226-390	02 28 12.3	-38 49 21	14330	52.9×46.9	46.9	42.8×12.9	10.9	22.9×7.3	6.4	AG674
MRK 605	03 15 37.3	-03 28 11	8410	51.1×46.7	-21.9	18.5×14.8	50.6	12.0×8.6	48.3	AG674
Tol 0614-375	06 16 13.8	-37 36 37	9893	65.1×46.2	31.1	42.1×16.0	-20.3	26.9×7.7	-22.8	AG674
Tol 0619-392	06 21 03.6	-39 17 07	1588	57.3×48.2	-44.5	46.1×14.4	-14.9	25.0×8.3	-10.7	AG674
MRK 711	09 55 11.4	+13 25 46	5756	57.0×49.4	44.1	32.2×14.3	-70.8	20.6×7.7	-68.5	AG674
Tol 0957-278	09 59 21.2	-28 08 00	710	74.1×53.0	-36.6	10.3×2.2	-50.3	40.9×10.6	-46.8	AS412,AG674
MRK 36	11 04 58.5	+29 08 22	646	53.7×50.0	76.7	4.4×4.2	13.4	8.4×8.2	48.7	AK331,AS734
Tol 1116-325	11 18 28.7	-32 53 10	600	92.4×85.7	14.4	33.8×16.9	6.8	17.7×9.4	-0.8	AG674
UM 421	11 20 10.7	-00 16 32	12039	58.0×47.8	28.2	46.6×14.4	-61.0	30.0×8.1	-60.1	AG674
UM 444	11 40 13.2	-00 24 42	6598	55.3×50.0	-25.9	47.4×14.3	-58.6	24.6×8.6	-61.7	AG674
UM 468	11 55 59.2	-01 00 01	10931	57.8×47.7	-13.3	40.6×14.6	-61.4	26.1×8.7	-61.1	AG674
UM 482	12 12 03.3	-00 36 22	10571	50.0×47.3	24.1	41.4×14.9	-62.0	21.3×8.7	-65.0	AG674
MRK 1315	12 15 18.7	+20 25 03	847	75.5×49.3	-73.7	1.4×1.2	-60.9	17.0×8.1	-75.4	AS286,AG674
MRK 1318	12 19 09.9	+03 51 21	1526	53.5×46.8	-2.2	4.8×4.3	5.7	3.0×2.5	43.9	AR541
UM 488	12 18 26.7	-00 07 50	15115	52.7×48.9	58.5	30.7×15.8	-69.1	16.6×9.1	-71.8	AG674
MRK 52	12 25 42.8	+00 34 22	2140	52.6×50.1	-1.4	5.4×4.5	-14.0	16.8×9.5	-72.5	AW137,AG67
Tol 1223-388	12 26 09.8	-39 07 26	3661	49.1×45.3	24.1	46.4×15.0	-11.4	26.4×8.8	-11.4	AG674
Tol 1247-232	12 50 18.9	-23 33 58	14390	51.6×47.2	40.1	25.0×18.9	-6.1	13.9×11.0	9.9	AG674
UM 530	12 58 08.4	+01 51 44	20019	60.7×59.7	-9.7	28.3×16.2	-70.2	17.7×9.0	-71.3	AG674
UM 533	12 59 58.1	+02 02 59	886	84.4×49.9	16.4	27.7×16.1	-73.2	15.0×9.1	-79.2	AG674
Tol 1303-281	13 05 43.7	-28 25 03	1499	49.7×48.9	-4.1	28.6×18.1	6.1	15.5×9.8	-4.5	AG674
Tol 1304-386	13 07 21.0	-38 54 49	4197	48.1×45.7	16.2	42.3×13.7	-3.1	24.0×8.8	2.2	AG674
Tol 1324-276	13 27 06.6	-27 57 23	2023	53.4×46.9	23.0	2.5×1.1	-2.9	1.5×0.6	4.1	AK431
UM 603	13 41 37.7	-00 25 55	17988	94.3×53.5	17.3	22.2×15.6	57.6	18.1×9.4	62.9	AG674
Tol 1358-328	14 01 21.6	-33 03 50	1216	106.8×82.4	14.2	31.9×16.3	2.9	17.8×9.8	-5.4	AG674
Tol 2259-398	23 02 22.5	-39 33 32	8858	55.1×47.4	34.8	44.9×12.3	4.9	25.0×7.3	9.9	AG674
Tol 2306-400	23 08 59.6	-39 45 51	19487	75.0×62.1	-12.0	51.1×12.8	17.3	25.7×7.4	12.6	AG674
MRK 930	23 31 58.3	+28 56 50	5485	53.7×48.2	-70.8	1.6×1.2	-43.4	9.5×7.6	63.8	AS314,AG674

[a]AG674 corresponds to our observations. In the case when observations were obtained from 2 different programs, the first one listed correspon to 4.9 GHz and the second one to 8.4 GHz.

Table 2. Radio properties of our sample

Name	F(1.4 GHz) (mJy)	F(4.9 GHz) (mJy)	F(8.4 GHz) (mJy)	$\alpha_5^{1.4}$	α_8^5	Comments
UM 304	6.43 ± 0.52	4.14 ± 0.12	2.85 ± 0.10	-0.35 ± 0.16	-0.68 ± 0.19	
Tol 0127-397	<1.47	0.67 ± 0.13	0.99 ± 0.06	>-0.65	···	a
Tol 0145-391	<1.41	<0.35	<0.27	···	···	
Tol 0226-390	3.73 ± 0.48	2.36 ± 0.13	1.69 ± 0.09	-0.37 ± 0.26	-0.61 ± 0.33	
MRK 605	<1.59	1.15 ± 0.07	0.85 ± 0.05	>-0.27	-0.55 ± 0.36	
Tol 0614-375	<1.74	<0.50	<0.25	···	···	
Tol 0619-392	<1.56	2.35 ± 0.23	1.32 ± 0.15	> 0.34	-1.05 ± 0.62	
MRK 711	2.64 ± 0.44	1.72 ± 0.19	1.39 ± 0.07	-0.34 ± 0.37	-0.39 ± 0.52	
Tol 0957-278	6.01 ± 0.51	2.00 ± 0.12	2.43 ± 0.12	···	···	b
MRK 36	2.41 ± 0.53	1.54 ± 0.08	0.78 ± 0.05	···	-1.24 ± 0.33	c
Tol 1116-325	<1.71	<0.31	<0.18	···	···	
UM 421	4.28 ± 0.50	2.32 ± 0.16	1.32 ± 0.11	-0.49 ± 0.25	-1.03 ± 0.44	
UM 444	<1.44	1.45 ± 0.14	1.00 ± 0.10	> 0.01	-0.68 ± 0.60	
UM 468	4.54 ± 0.51	2.17 ± 0.11	1.24 ± 0.08	-0.59 ± 0.23	-1.02 ± 0.36	
UM 482	<1.44	<0.35	<0.25	···	···	
MRK 1315	<1.41	0.56 ± 0.11	0.90 ± 0.08	···	···	b
MRK 1318	<1.44	0.83 ± 0.06	0.83 ± 0.03	>-0.46	0.00 ± 0.34	
UM 488	3.73 ± 0.51	1.33 ± 0.10	0.82 ± 0.08	-0.83 ± 0.28	-0.88 ± 0.51	
MRK 52	13.21± 0.45	4.27 ± 0.13	4.44 ± 0.09	···	···	b
Tol 1223-388	<1.56	2.39 ± 0.18	1.49 ± 0.17	> 0.35	-0.86 ± 0.58	
Tol 1247-232	3.27 ± 0.57	2.29 ± 0.13	1.45 ± 0.11	-0.29 ± 0.34	-0.83 ± 0.39	
UM 530	6.43 ± 0.45	2.27 ± 0.10	1.64 ± 0.08	-0.83 ± 0.15	-0.59 ± 0.28	
UM 533	2.63 ± 0.44	5.29 ± 0.08	4.19 ± 0.07	0.56 ± 0.31	-0.43 ± 0.09	
Tol 1303-281	<1.38	<0.71	<0.35	···	···	
Tol 1304-386	<1.47	1.33 ± 0.22	0.99 ± 0.17	>-0.08	-0.54 ± 0.98	
Tol 1324-276	3.90 ± 0.47	0.78 ± 0.04	0.51 ± 0.03	···	-0.78 ± 0.33	c
UM 603	3.74 ± 0.51	1.38 ± 0.09	0.98 ± 0.08	-0.80 ± 0.28	-0.62 ± 0.42	
Tol 1358-328	<1.71	3.40 ± 0.17	2.47 ± 0.13	> 0.57	-0.58 ± 0.30	
Tol 2259-398	<1.77	1.49 ± 0.14	0.84 ± 0.09	>-0.14	-1.05 ± 0.62	
Tol 2306-400	<1.38	0.92 ± 0.12	0.84 ± 0.10	>-0.34	-0.17 ± 0.74	
MRK 930	11.53± 0.48	2.72 ± 0.09	3.66 ± 0.05	···	···	b

·Flux upper limits and $\alpha_5^{1.4}$ lower limits are defined as three times the image r.m.s. level.

[a]Observations at 1.4 GHz and 4.9 GHz were obtained with similar resolution, but 8.4 GHz was observed with too high a resolution to allow a reliable determination of α_8^5.

[b]Observations taken with different resolutions to allow the reliable determination of any spectral index.

[c]Observations taken with similar resolution at 4.9 GHz and 8.4 GHz, but not at 1.4 GHz, so $\alpha_5^{1.4}$ cannot be reliably determined.

Table 3. Optical properties and SFRs of our sample

Name	Log F(Hα)	Log F(Hβ)	EW(Hβ)	A_v	[OIII]/Hβ	SFR(Hα)	SFR(1.4 GHz)	Log L(Hα)	Log Mass
	(erg s^{-1} cm^{-2})		(Å)			($M_\odot year^{-1}$)		(erg s^{-1})	($M_\odot$)
UM 304	-12.47	-12.92	18	2.33	1.31	2.1	2.1	41.28	6.78
Tol 0127-397	-12.38	-12.83	38	1.09	3.28	2.6	0.5	41.38	6.88
Tol 0145-391	-11.34	-11.80	24	0.01	0.94	312.2	< 5.1	43.45	8.95
Tol 0226-390	-12.32	-12.78	106	0.99	5.24	25.5	10.7	42.36	7.86
MRK605	-12.21	-12.66	7	2.87	0.81	13.5	1.9	42.09	7.59
Tol 0614-375	-12.33	-12.79	8	2.68	0.87	12.2	< 2.5	42.05	7.55
Tol 0619-392	-12.17	-12.62	15	2.76	1.91	46.0	5.7	42.62	8.12
MRK711	-12.52	-12.98	36	0.82	2.75	2.6	1.2	41.38	6.88
Tol 0957-278	-12.33	-12.79	29	1.02	4.20	0.3	< 0.2	40.41	5.91
MRK36	-12.45	-12.91	70	0.96	5.68	0.1	< 0.1	39.84	5.34
Tol 1116-325	-12.43	-12.89	264	1.07	5.25	0.04	< 0.1	39.51	5.01
UM 421	-12.19	-12.64	5	4.24	1.58	25.0	8.9	42.35	7.85
UM 444	-12.24	-12.70	29	1.69	3.23	7.9	1.1	41.85	7.35
UM 468	-12.52	-12.97	27	1.26	3.11	10.1	8.1	41.97	7.47
UM 482	-12.49	-12.94	24	1.49	3.06	10.2	< 2.4	41.96	7.46
MRK1315	-12.55	-13.01	391	0.01	5.73	0.03	< 0.1	39.40	4.90
MRK1318	-12.44	-12.90	121	0.40	3.63	0.2	< 0.1	40.30	5.80
UM 488	-12.31	-12.76	14	2.33	2.13	30.9	12.6	42.45	7.95
MRK52	-10.89	-11.34	29	3.06	0.84	19.9	< 1.1	42.26	7.76
Tol 1223-388	-12.52	-12.97	35	1.21	0.83	0.9	0.2	40.91	6.41
Tol 1247-232	-12.07	-12.53	97	0.74	5.37	47.4	9.8	42.63	8.13
UM 530	-11.92	-12.37	28	2.12	2.50	143.9	40.9	43.12	8.62
UM 533	-12.36	-12.82	101	1.66	4.87	0.2	0.1	40.19	5.69
Tol 1303-281	-12.39	-12.84	161	1.15	6.16	0.2	< 0.1	40.35	5.85
Tol 1304-386	-12.50	-12.96	286	0.67	6.89	1.5	0.4	41.13	6.63
Tol 1324-276	-12.43	-12.88	113	0.49	5.66	0.3	< 0.2	40.47	5.97
UM 603	-12.52	-12.98	23	1.64	1.75	20.4	13.6	42.27	7.77
Tol 1358-328	-12.29	-12.75	166	0.37	4.27	0.1	< 0.1	40.01	5.51
Tol 2259-398	-12.01	-12.46	25	2.25	1.46	19.9	1.9	42.26	7.76
Tol 2306-400	-11.88	-12.33	7	3.71	1.49	135.6	7.6	43.09	8.59
MRK930	-12.03	-12.49	71	1.20	3.35	7.2	< 4.8	41.82	7.32

·Column 1: name of the galaxy; Columns 2 and 3: Logarithm of the extinction corrected Hα and Hβ emission lines fluxes; Column 4: observed Hβ equivalent width; Column 5: visual extinction; Column 6:[OIII]/Hβ; Columns 7: extiction corrected SFR(Hα); Column 8: SFR(1.4GHz); Column 9: Log L(Hα); Column 10: Mass of the burst from SB99 (see text).

Table 4. Infrared fluxes, d and q parameters for our sample

Name	d %	F(60 μm) (Jy)	F(100 μm) (Jy)	q
UM 304	100	1.983	2.426	2.6
Tol 0127-397	$<$ 19	0.233	$<$0.351	$>$ 2.6
Tol 0145-391	$<$ 5	–	–	–
Tol 0226-390	42	0.791	0.480	2.4
MRK605	$<$ 14	0.272	$<$1.359	$>$ 2.6
Tol 0614-375	$<$ 61	0.216	$<$0.529	$>$ 2.0
Tol 0619-392	$<$ 12	0.419	$<$1.587	$>$ 2.8
MRK711	47	0.809	0.749	2.6
Tol 0957-278	70	–	–	–
MRK36	37	0.225	$<$0.681	2.1
Tol 1116-325	$<$ 75	–	–	–
UM 421	35	0.560	$<$1.304	2.3
UM 444	$<$ 14	–	–	–
UM 468	80	0.295	0.589	2.0
UM 482	$<$ 71	–	–	–
MRK1315	$<$ 81	–	–	–
MRK1318	$<$ 22	0.730	0.940	$>$ 2.8
UM 488	40	–	–	–
MRK52	5	4.430	6.650	2.7
Tol 1223-388	$<$ 27	1.140	2.534	$>$ 3.1
Tol 1247-232	21	0.507	$<$0.968	2.3
UM 530	28	0.576	0.632	2.0
UM 533	33	0.496	0.540	2.4
Tol 1303-281	$<$ 54	–	–	–
Tol 1304-386	$<$ 25	–	–	–
Tol 1324-276	56	0.557	0.740	2.3
UM 603	67	–	–	–
Tol 1358-328	$<$ 18	1.563	2.704	$>$ 3.1
Tol 2259-398	$<$ 10	–	–	–
Tol 2306-400	$<$ 6	–	–	–
MRK930	67	1.245	$<$2.154	2.2

·Column 1: Name of the galaxy; Column 2: d-parameter; Columns 3 and 4: IRAS fluxes at 60 μm and 100 μm; Column 5 q parameter.

Table 5. Star formation rate and d parameter of normal galaxies

Name	cz (km/s)	EW(Hβ) (Å)	SFR(Hα) ($M_\odot year^{-1}$)	F(1.4 GHz) (mJy)	SFR(1.4 GHz) ($M_\odot year^{-1}$)	d parameter (%)	Ref.
UGC00484	4859	4.3	2.7	4.4	1.5	56	1
UGC01154	7756	6.0	5.8	5.6	5.0	88	1
UGC01155	3158	7.5	0.7	4.4	0.6	92	1
NGC695	9705	0.8	79.4	75.6	107.2	135	1
UGC01551	2669	5.6	0.8	3.0	0.3	38	1
IC197	6332	0.8	3.8	10.9	6.5	171	1
UGC01630	4405	6.2	2.5	14.3	4.1	163	1
NGC927	8258	1.0	10.2	16.7	17.0	166	1
UGC04713	9036	0.8	19.5	2.9	3.5	18	1
NGC2844	1486	1.7	0.1	3.9	0.1	89	1
NGC3011	1517	4.2	0.05	3.0	0.1	200	1
IC2520	1226	0.8	0.5	24.1	0.5	109	1
NGC3075	3566	6.0	0.7	3.9	0.7	102	1
NGC3104	604	10.4	0.04	1.8	0.01	23	1
NGC3264	929	20.5	0.11	2.1	0.03	23	1
NGC3279	1422	1.9	0.3	8.7	0.3	101	1
UGC05744	3338	5.8	0.6	5.1	0.8	134	1
UGC05760	2997	4.7	0.8	7.9	1.0	126	1
IC2591	6755	1.1	2.7	5.3	3.6	134	1
UGC05819	10693	0.3	2.3	5.4	9.3	402	1
NGC3510	704	13.4	0.07	3.1	0.02	31	1
IC673	3851	1.8	1.1	5.6	1.2	105	1
NGC3633	2553	2.8	1.7	19.4	1.9	107	1
UGC06625	10964	7.4	11.0	17.4	31.6	287	1
IC746	5027	1.3	1.3	4.4	1.7	131	1
NGC3978	9978	5.2	21.4	38.2	57.5	270	1
UGC07020A	1447	12.4	0.3	5.3	0.2	45	1
NGC4120	2251	8.7	0.3	4.0	0.3	98	1
NGC4159	1761	8.8	0.3	5.9	0.3	83	1
NGC4238	2771	10.2	0.5	3.2	0.4	68	1
UGC07358	3639	3.9	0.8	3.2	0.6	79	1
UGC07690	540	7.6	0.02	1.6	0.01	33	1
NGC4509	907	25.0	0.1	2.8	0.03	36	1
UGC07761	6959	5.9	4.3	8.9	6.5	151	1
NGC4758	1244	3.5	0.2	3.0	0.07	35	1
NGC5230	6855	4.3	8.7	19.5	13.8	158	1
UGC08630	2364	9.7	0.3	3.0	0.2	84	1
NGC5425	2062	4.9	0.2	7.1	0.4	182	1
NGC5491	5845	1.9	2.9	4.7	2.4	81	1
NGC5541	7698	4.8	10.2	33.0	29.5	284	1
UGC09356	2234	5.9	0.2	2.5	0.2	75	1
UGC09560	1215	45.9	0.2	5.9	0.1	84	1
IC1100	6561	0.9	3.6	7.6	4.9	134	1

Table 5—Continued

Name	cz (km/s)	EW(Hβ) (Å)	SFR(Hα) ($M_\odot year^{-1}$)	F(1.4 GHz) (mJy)	SFR(1.4 GHz) ($M_\odot year^{-1}$)	d parameter (%)	Ref.
IC1124	5242	0.9	2.6	3.1	1.3	48	1
IC1141	4458	0.3	1.3	10.7	3.2	230	1
NGC6007	10548	3.3	7.8	13.5	22.9	292	1
UGC10086	2191	10.3	0.3	3.9	0.3	108	1
NGC6131	5054	4.2	1.0	6.5	2.5	247	1
NGC7328	2827	1.9	1.4	6.9	0.8	58	1
UGC12178	1925	3.6	0.4	7.2	0.4	96	1
UGC12265	5682	12.9	3.2	14.1	6.8	208	1
NGC7460	3296	5.9	2.6	13.3	2.1	81	1
UGC12519	4380	6.2	2.2	4.6	1.3	57	1
NGC7620	9565	7.1	31.6	31.5	43.7	139	1
IC1504	6306	1.7	11.2	7.4	4.4	38	1
NGC2782	2558	6.9	6.6	124.5	12.2	185	2
NGC3310	988	21.0	7.6	396.9	9.8	128	2
NGC3367	3041	6.2	9.7	117.6	15.8	162	2
NGC3432	615	11.1	0.5	83.3	0.4	73	2
NGC3504	1538	5.7	6.8	274.1	13.6	199	2
NGC3690	3033	21.8	33.3	686.3	79.1	237	2
NGC3893	971	5.7	4.0	139.2	2.8	70	2
NGC3949	796	7.2	2.5	118.4	2.4	97	2
NGC4088	759	5.9	4.5	222.0	4.5	99	2
NGC4102	837	2.3	2.7	272.7	5.6	205	2
NGC4157	775	3.5	2.1	190.0	3.9	182	2
NGC4214	291	20.9	0.2	37.2	0.03	14	2
NGC4217	1026	1.3	1.1	120.3	2.5	229	2
NGC4254	2406	6.1	8.7	447.4	8.9	102	2
NGC4303	1569	6.3	5.3	444.3	7.2	137	2
NGC5676	2116	3.8	11.2	113.7	9.6	84	2

·Column 1: Galaxy Name; Column 2: redshift; Column 3: Hβ equivalent width; Column 4: Hα SFR; Column 5: 1.4 GHz flux; Column 6: 1.4 GHz SFR; Column 7: d-parameter; Column 8: reference from which the galaxy was obtained (1- Jansen et al. 2000; 2- Ho et al. 1997)

Table 6. Radio and Infrared properties of galaxies from Ho et al. (1997)

Name	Type	Distance	F(1.4 GHz) (mJy)	F(4.8 GHz) (mJy)	F(60 μm) (Jy)	F(100 μm) (Jy)	q	References
NGC2782	1	37.3	124.5±5.1	49± 8	9.60	14.65	2.03	1
NGC2964	4	21.9	105.2±3.9	33± 6	12.47	24.14	2.25	1
NGC2967	5	30.9	111.5±3.7	49± 11	5.81	15.12	1.96	2
NGC3310	4	18.7	396.9±12.5	152± 17	34.13	47.95	2.06	1
NGC3367	5	43.6	117.6±4.2	36± 8	6.06	12.49	1.91	1
NGC3432	9	7.8	83.3±3.4	40± 7	8.55	16.44	2.19	1
NGC3504	2	26.5	274.1±10.6	117± 16	22.70	35.70	2.06	1
NGC3556	6	14.1	284.1±8.0	76± 9	32.19	80.77	2.29	1
NGC3583	3	34.0	59.2±2.4	30± 6	7.18	19.50	2.33	1
NGC3593	0	5.5	86.2±3.4	55± 10	18.27	36.00	2.51	1
NGC3631	5	21.6	84.0±3.5	31± 6	9.58	26.77	2.31	1
NGC3690	9	40.4	686.3±26.5	300± 4	121.64	122.45	2.33	4
NGC3810	5	16.9	124.3±4.7	46± 9	13.99	35.08	2.28	1
NGC3893	5	17.0	139.2±5.0	39± 7	15.07	39.26	2.28	1
NGC3949	4	17.0	118.4±4.2	37± 6	11.37	26.52	2.20	1
NGC4088	4	17.0	222.0±6.3	67± 9	26.56	60.83	2.29	1
NGC4102	3	17.0	272.7±9.6	70± 9	50.56	75.72	2.40	1
NGC4157	3	17.0	190.0±6.4	60± 8	17.65	49.95	2.23	1
NGC4214	10	3.5	37.2±1.8	30± 7	17.87	29.04	2.83	1
NGC4217	3	17.0	120.3±4.3	40± 7	11.70	41.40	2.30	1
NGC4254	5	16.8	447.4±12.2	111± 16	44.00	96.32	2.20	1
NGC4303	4	15.2	444.3±13.6	157± 23	41.00	77.40	2.14	1
NGC4449	10	3.0	264.0±7.2	108± 13	37.00	58.28	2.29	1
NGC4490	7	7.8	807.9±20.8	226± 27	47.79	85.94	1.94	1
NGC4532	10	15.5	122.8±4.3	54± 10	10.00	14.88	2.05	1
NGC4535	5	16.8	77.6±5.3	38± 9	14.00	31.82	2.47	1
NGC4536	4	13.3	205.1±7.7	114± 12	28.66	44.63	2.29	1
NGC4631	7	6.9	976.2±16.7	438± 66	82.90	208.66	2.16	3
NGC4654	6	16.8	122.5±4.6	48± 9	14.70	34.40	2.30	1
NGC4793	5	38.9	113.3±4.1	46± 8	12.88	29.28	2.27	1
NGC5248	4	22.7	157.4±7.0	71± 12	20.71	49.08	2.34	1
NGC5676	4	34.5	113.7±4.2	38± 6	12.45	31.55	2.27	1
NGC5775	5	26.7	279.9±9.1	67± 12	23.41	51.35	2.13	1
NGC5907	5	14.9	103.4±3.8	38± 6	8.78	45.76	2.35	1
NGC5962	5	31.8	83.8±3.2	36± 8	8.99	20.79	2.25	1
NGC6181	5	36.7	95.6±3.5	56± 9	9.35	21.00	2.20	1

·The 1.4 GHz fluxes are from the NVSS catalogue and the references for the fluxes at 4.8 GHz are in column 8: 1- Gregory & Condon (1991), 2- Griffith, M. R., et al. (1995), 3- Becker, White & Edwards (1991) and 4- Condon, Anderson & Broderick (1995).

Table 7. Tracers of a very young star forming episode

Name	High EW(Hβ) $\geqslant 70$ Å	High OIII/Hβ $\geqslant 2$	High $\alpha_5^{1.4}$ > -0.5	Low d $\leqslant 75$ %	High q > 2.5
UM 304	X	X	√	X	√
Tol 0127-397	X	√	X	√	√
Tol 0145-391	X	X	–	√	–
Tol 0226-390	√	√	√	√	X
MRK605	X	X	√	√	√
Tol 0614-375	X	X	–	√	?
Tol 0619-392	X	X	√	√	√
MRK711	X	√	√	√	√
Tol 0957-278	X	√	–	√	–
MRK36	√	√	–	√	X
Tol 1116-325	√	√	–	√	–
UM 421	X	X	√	√	X
UM 444	X	√	√	√	–
UM 468	X	√	X	X	X
UM 482	X	√	–	√	–
MRK1315	√	√	–	?	–
MRK1318	√	√	√	√	√
UM 488	X	√	X	√	–
MRK52	X	X	–	√	√
Tol 1223-388	X	X	√	√	√
Tol 1247-232	√	√	√	√	X
UM 530	X	√	X	√	X
UM 533	√	√	√	√	X
Tol 1303-281	√	√	–	√	–
Tol 1304-386	√	√	√	√	–
Tol 1324-276	√	√	–	√	X
UM 603	X	X	X	√	–
Tol 1358-328	√	√	√	√	√
Tol 2259-398	X	X	√	√	–
Tol 2306-400	X	X	√	√	–
MRK930	√	√	–	√	X